iScience

CellPress

Article

Near-Infrared-Detached Adhesion Enabled by Upconverting Nanoparticles

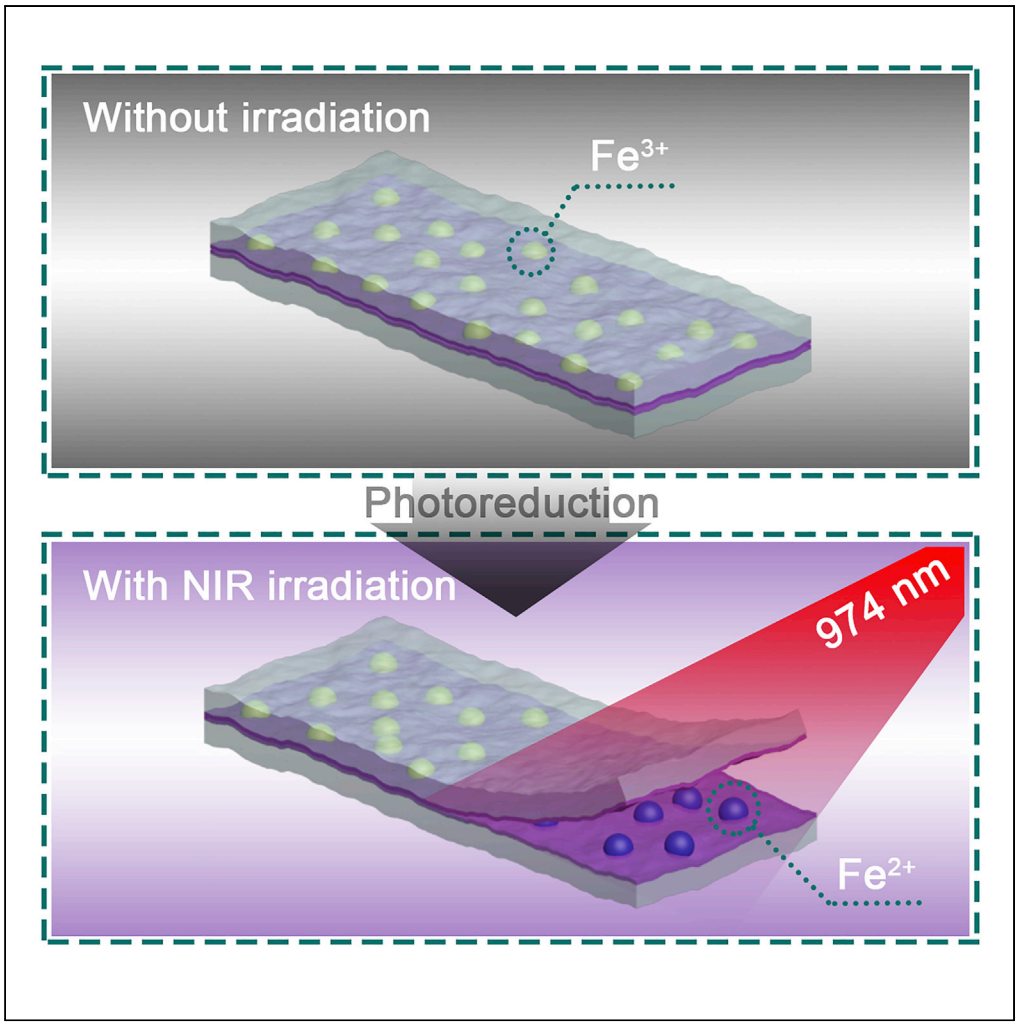

Mingyue Jiang, Xue Liu, Zhijun Chen, Jian Li, Shouxin Liu, Shujun Li

chenzhijun@nefu.edu.cn (Z.C.)
lishujun@nefu.edu.cn (S.L.)

HIGHLIGHTS

NIR-detached adhesion assisted by upconverting nanoparticles was developed

As-developed NIR-detached adhesion was applicable in deep tissue

Formula for NIR-detached adhesion showed good biocompatibility

Jiang et al., iScience *23*, 100832
February 21, 2020
https://doi.org/10.1016/j.isci.2020.100832

iScience

CellPress

Article

Near-Infrared-Detached Adhesion Enabled by Upconverting Nanoparticles

Mingyue Jiang,[1] Xue Liu,[1] Zhijun Chen,[1,2,*] Jian Li,[1] Shouxin Liu,[1] and Shujun Li[1,*]

SUMMARY

Achieving efficient and biocompatible detachment between adhered wet materials (i.e., tissues and hydrogels) is a major challenge. Recently, photodetachable topological adhesion has shown great promise as a strategy for conquering this hurdle. However, this photodetachment was triggered by UV light with poor biocompatibility and penetration capacity. This study describes near-infrared (NIR) light-detached topological adhesion based on polyacrylic acid coated upconverting nanoparticles (UCNP@PAA) and a photodetachable adhesive (termed Cell-Fe). Cell-Fe is a coordinated topological adhesive consisting of carboxymethylcellulose and Fe^{3+} that can be photodecomposed by UV light. To prepare a substrate for NIR-detached topological adhesion, UCNP@PAA and Cell-Fe were mixed and brushed on the surface of the model adherent. The UCNP@PAA can harvest NIR light and convert it into UV light, triggering the decomposition of the Cell-Fe and inducing the detachment. This NIR-detached topological adhesion is also feasible in deep tissue because of the ability of NIR light to penetrate tissue.

INTRODUCTION

Adhesion between wet materials (i.e., tissues and hydrogels) has broad applications, including in tissue repair, wound dressing, wearable electronic devices and drug delivery (Yang et al., 2018; Li et al., 2017; Li and Mooney, 2016). For some expensive and biological adherents, non-invasive on-demand detachment is necessary, but it is not easily achieved with traditional adhesives (Yang et al., 2018; Li et al., 2017; Li and Mooney, 2016). Detachable topological adhesion is an attractive solution to this problem (Yu et al., 2011). Topological adhesion, specifically topological entanglement with the two preexisting molecular networks, involves the diffusion of polymer chains into the two preexisting molecular networks, forming a third polymer network *in situ* due to cross-linking (Steck et al., 2019). As a result, the breaking of the topological adhesion via detachment requires the breaking of the third network formed by the diffused polymer chains (Sun et al., 2013; Xu et al., 2010). Several methods, such as pH (Yang et al., 2018), thermo (Luo et al., 2010), and light (Kamperman and Synytska, 2012), have been developed to detach topological adherents. Light shows promise in detaching topological adherents as it can provide spatiotemporal control (Xu et al., 2018; Guimard et al., 2012). However, photodisrupted topological adhesion has only been achieved by using UV light, which is problematic because its high-energy photons can damage DNA and important chemical bonds (Wang et al., 2017). Moreover, UV photons cannot deeply penetrate tissue, which might limit their applications in thick and macroscopic adherents (Strehmel and Strehmel, 2007). To solve these problems, we turned our attention to near-infrared (NIR) light. NIR light can deeply penetrate guest materials while causing less photodamage to chemical bonds and biological systems (Lederhose et al., 2016). Recently, NIR light-triggered photoreactions based on upconverting nanoparticles have been developed (Wu et al., 2016; Yan et al., 2012; Carling et al., 2009; Chen et al., 2014a, 2014b). Upconverting nanoparticles can convert NIR light into UV and visible light (Chen et al., 2015a, 2015b; Chan et al., 2012; Wu et al., 2016; Huang et al., 2016; Li et al., 2013; Tian et al., 2013; All et al., 2019). Then, the upconverted UV or visible emission can trigger photoreactions of traditional UV- or visible light-responsive compounds. This process is referred to as upconverting nanoparticle-assisted photochemistry (Wu and Butt, 2016; Yang et al., 2012, 2015; Viger et al., 2013; Wu et al., 2011; Ruggiero et al., 2014; Burks et al., 2013). Upconverting nanoparticles have facilitated different photoreactions, including photoisomerization (Wu and Yao, 2011; Li et al., 2014), photocleavage (Yan et al., 2011; Zhao et al., 2014), photopolymerization (Yang et al., 2012; Stepuk et al., 2012), and photocoupling (Lederhose et al., 2016). These upconverting nanoparticle-assisted photoreactions have been applied to NIR-controlled biointerfaces (Li et al., 2014; Chen et al., 2015a, 2015b), catalysis (Chen et al., 2014a, 2014b), uncaging enzymes (Gao et al., 2015), drug delivery (Yang et al., 2015; He et al., 2015), pH adjustments (Chen et al., 2016), and actuators (Wu and Yao, 2011). Here, we use NIR light to detach a topological adherent based on upconverting nanoparticle-assisted photochemistry (Figure 1).

[1]Key Laboratory of Bio-based Material Science and Technology of Ministry of Education, Northeast Forestry University, Hexing Road 26, Harbin 150040, P.R. China

[2]Lead Contact

*Correspondence: chenzhijun@nefu.edu.cn (Z.C.), lishujun@nefu.edu.cn (S.L.)

https://doi.org/10.1016/j.isci.2020.100832

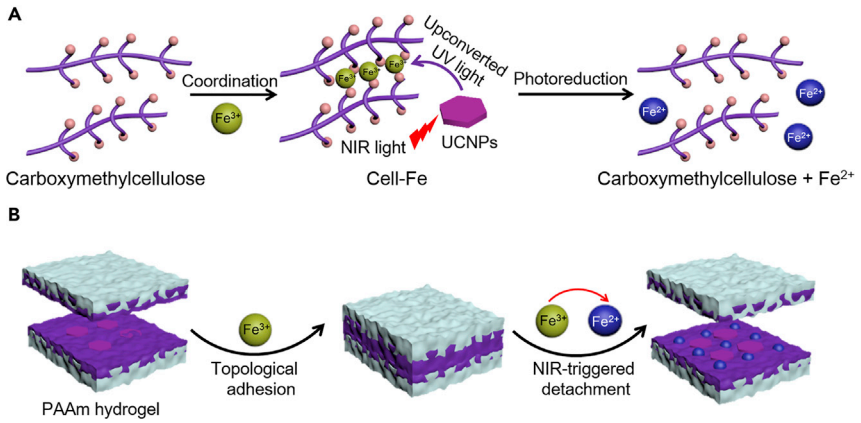

Figure 1. Schematic Illustration of NIR-Detached Adhesion Enabled by Upconverting Nanoparticles

(A) Schematic of the coordination between carboxymethylcellulose and Fe^{3+} and NIR-triggered photoreduction assisted by the UCNP@PAA.

(B) Topological adhesion and NIR-disrupted topological adhesion between hydrogels based on UCNP-assisted photoreduction.

We refer to this new method as photon upconversion topological adhesion detachment (PUTAD). To construct a platform for PUTAD, water-soluble $NaYF_4$:TmYb@$NaYF_4$@PAA upconverting nanoparticles (UCNP@PAA) and photodetachable adhesives (Cell-Fe) were prepared. In this study, topological adhesion was first achieved to a model adherent (polyacrylamide [PAAm] hydrogel) using UCNP@PAA-doped Cell-Fe adhesives via coordination between Fe^{3+} and carboxymethylcellulose. Upon NIR irradiation, UCNP@PAA can convert NIR light to UV light, which photoreduces Fe^{3+} to Fe^{2+} and disrupts the coordination (Figure 1). As a result, the adherent was detached from the hydrogel. Moreover, the as-developed PUTAD demonstrated effective photodetachment in deep tissue. NIR could penetrate 3-mm-thick tissue and trigger detachment between the hydrogel and tissue.

RESULTS

$NaYF_4$:TmYb@$NaYF_4$ upconverting nanoparticles with an average diameter of 50 nm were synthesized according to our previous work (Figure 2A) (Chen et al., 2015b). To prepare water-soluble UCNPs, polyacrylic acid (PAA) was used to coat the hydrophobic surface of the UCNPs. In this manner, UCNP@PAA with suitable water solubility were synthesized (Figures 2B and 2C). These UCNP@PAA emitted blue light under 974-nm NIR light excitation (Chen et al., 2015b). The absorption band of Cell-Fe was between those of carboxymethylcellulose and Fe^{3+} in the UV light region and overlapped with the UV emission of the UCNP@PAA (Figure 2D). To demonstrate the absorption of the upconverted UV light by Cell-Fe, we compared the upconversion luminescence spectra of UCNP@PAA in the presence and absence of Cell-Fe. The intensity of the upconversion luminescence of UCNP@PAA at 360 nm was lower in the presence of Cell-Fe (Figures 2E and S1). A higher concentration of Cell-Fe absorbed more of the upconverted UV light, resulting in a lower emission intensity (Figure 2E). In contrast, the emission at 800 nm, a spectral region where Cell-Fe has no absorption, still remained (Figure S2). The transfer efficiency between UCNP@PAA (2 mg/mL) and Cell-Fe (Cell = 1 wt%, Fe^{3+} = 0.81 mg) was 51.5% according to the equation (Supplemental information Equation S1). This result suggested the efficient absorption of the upconverted UV light by Cell-Fe. Subsequently, the NIR-triggered reduction of Fe^{3+} through the assistance of UCNP@PAA was investigated (Figure 2F). Approximately 88% of Fe^{3+} was reduced to Fe^{2+} upon NIR irradiation for 100 min (Figure 2G). This spectral change was identical to that observed for Cell-Fe, which was directly photoreduced using UV light (Figure 2G). Thus, Cell-Fe was photocleaved by NIR light radiation. Exposing Cell-Fe to NIR light in the absence of UCNP@PAA did not obviously reduce Fe^{3+} (Figure S3), proving that the photon upconversion process was required for the photoreduction of Cell-Fe.

After that, an aqueous solution of carboxymethylcellulose chains was brushed on the surfaces of two pieces of polyacrylamide (PAAm) hydrogel, and the pieces were left to stand for some time to allow the carboxymethylcellulose chains to diffuse into the hydrogels. Subsequently, an aqueous solution of Fe^{3+} with citric

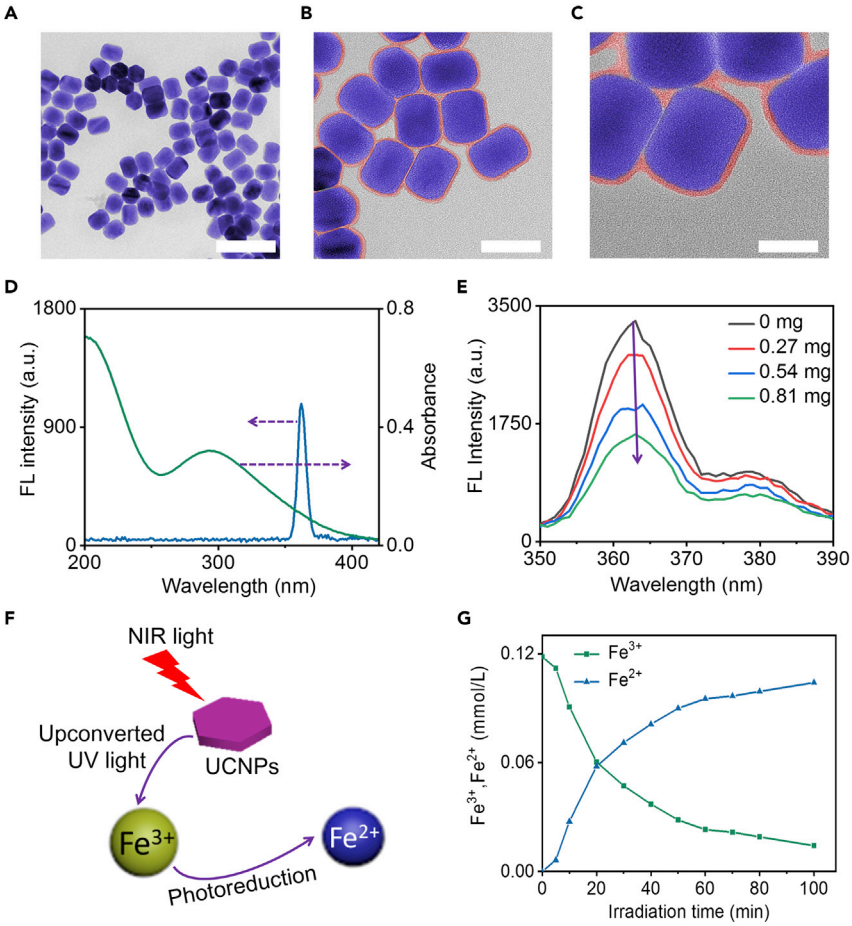

Figure 2. NIR-Triggered Photoreduction Assisted by UCNP@PAA

(A–C) TEM images of (A) UCNPs, scale bar: 100 nm; (B) UCNP@PAA, scale bar: 50 nm; and (C) UCNP@PAA, scale bar: 20 nm.

(D) Absorbance of Cell-Fe and fluorescence emission of UCNP@PAA.

(E) Fluorescence emission of UCNP@PAA (ranging from 350 to 390 nm) upon addition of Cell-Fe at different concentrations.

(F) Schematic of NIR-triggered photoreduction assisted by UCNP@PAA.

(G) Changes in the Fe^{3+}/Fe^{2+} concentrations upon NIR irradiation (1 W) in the presence of UCNP@PAA.

See also Figures S1–S3.

acid at a controlled pH (pH = 3) and UCNP@PAA was added to one piece of hydrogel, and the other piece of hydrogel was immediately pressed on top of the coated piece. The Fe^{3+} ions diffused into the hydrogel and formed coordination complexes with the carboxyl groups, which cross-linked into a carboxymethylcellulose network, resulting in topological entanglement with the two preexisting PAAm networks of the hydrogels. The strength of the topological adhesion was dynamically detected. After 60 min, the adhesion strength reached ~50 J m^{-2} (Figures 3A and S4). Having determined the topological adhesion, NIR-triggered photodetachment was investigated (Figures 3B and S5). Before NIR irradiation, SEM images of the interface of the two hydrogels were acquired. A dense interfacial zone ~0.5 μm thick formed between the two hydrogels (Figure 3C, left). Upon NIR irradiation, UCNP@PAA converted the NIR light to UV light, which photoreduced Fe^{3+} to Fe^{2+}. After that, the Fe^{3+}-cross-linked carboxymethylcellulose network dissociated, regenerating the polymer chains, and an obvious crack was observed (Figure 3C, right). The adhesion strength also decreased from ~60 to ~9 J m^{-2} upon NIR irradiation (Figure 3D). As a control, the adhesion strength did not show an obvious change without NIR irradiation (Figure 3D). To investigate the possible thermal effect on the detaching process, we used an IR camera to detect the temperature change during the detachment and ~6°C increase was observed (Figure S8). To check whether this photothermal effect contributed to the detachment, a control group in the absence of UCNP@PAA upon NIR

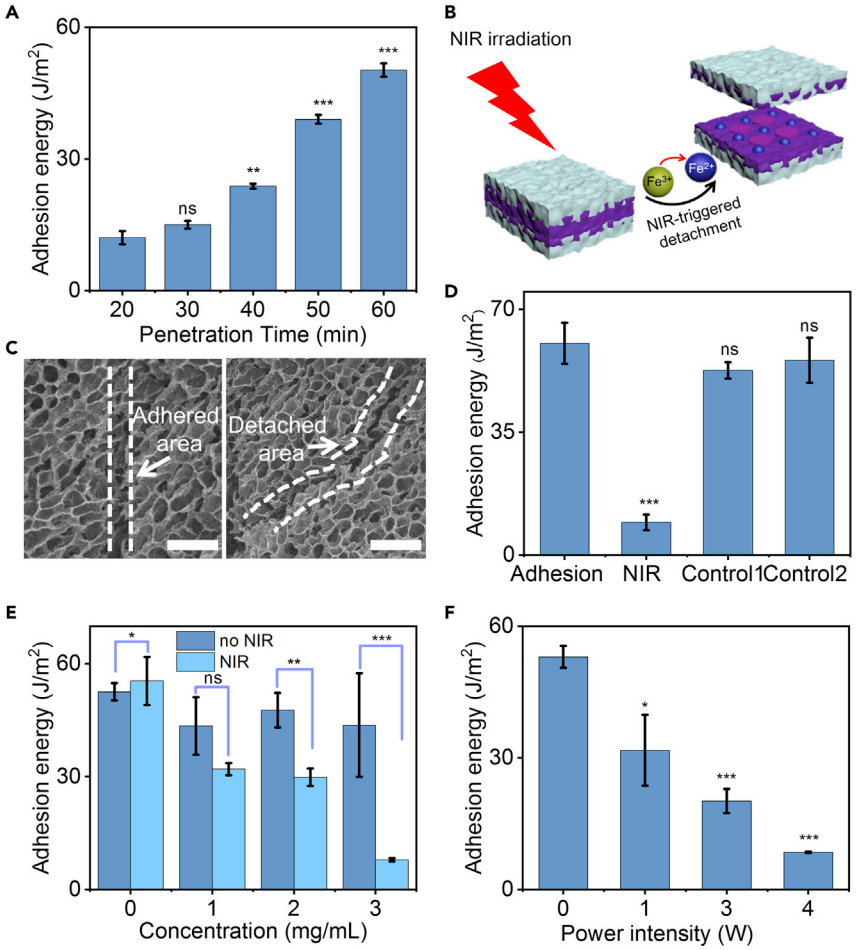

Figure 3. NIR-Detached Hydrogel Adesion Assisted by UCNP@PAA

(A) Strength of the topological adhesion between hydrogels at different times.

(B) Schematic of NIR-triggered detachment of topologically adhered hydrogels.

(C) SEM images of topological adhesion between hydrogels before (left) and after NIR irradiation (right); scale bar: 5 μm.

(D) Strength of the topological adhesion between hydrogels before and after NIR irradiation (NIR intensity = 4 W). Control 1: before irradiation with UCNP@PAA, Control 2: after irradiation without UCNP@PAA.

(E) Strength of the topological adhesion between hydrogels before and after NIR irradiation at different concentrations of UCNP@PAA (NIR intensity = 4 W, irradiation time = 5 min).

(F) Strength of the topological adhesion between hydrogels upon NIR irradiation at different intensities.

*$p < 0.05$, **$p < 0.01$, ***$p < 0.001$, ns = no statistical difference. See also Figures S4–S6 and S8.

excitation was added. The adhesion strength did not show obvious changes (Figure 3D). These results confirmed that the detachment was triggered by photon upconversion process rather than by photothermal effect. To make the detachment more obvious, a weight was attached to the glued hydrogel. The glued hydrogel was detached and the weight dropped upon NIR irradiation (Figure S6A and Video S1). While, no any change was observed without NIR irradiation (Figure S6B and Video S2). The photodetachment was closely related to the concentration of UCNP@PAA. Higher concentrations of UCNP@PAA triggered more obvious photodetachment of the hydrogels. When the concentration of UCNP@PAA in the adhesive formula was 3 mg/mL, NIR irradiation triggered a loss of ~80% of the adhesion strength (from ~42 to ~8 J m^{-2}, Figure 3E). The photodetachment of the hydrogels was also investigated upon NIR irradiation at different intensities. More obvious photodetachment was observed with higher-intensity NIR radiation. NIR irradiation at 1 W only triggered a 40% decrease in the adhesion strength (~53 to ~31 J m^{-2}, Figure 3F). In contrast, a loss of ~80% adhesion strength was observed upon NIR irradiation at 4 W (~53 to ~8.5 J m^{-2}, Figure 3F). These results demonstrated that an NIR source could be used to detach topological adherents in a well-controlled manner.

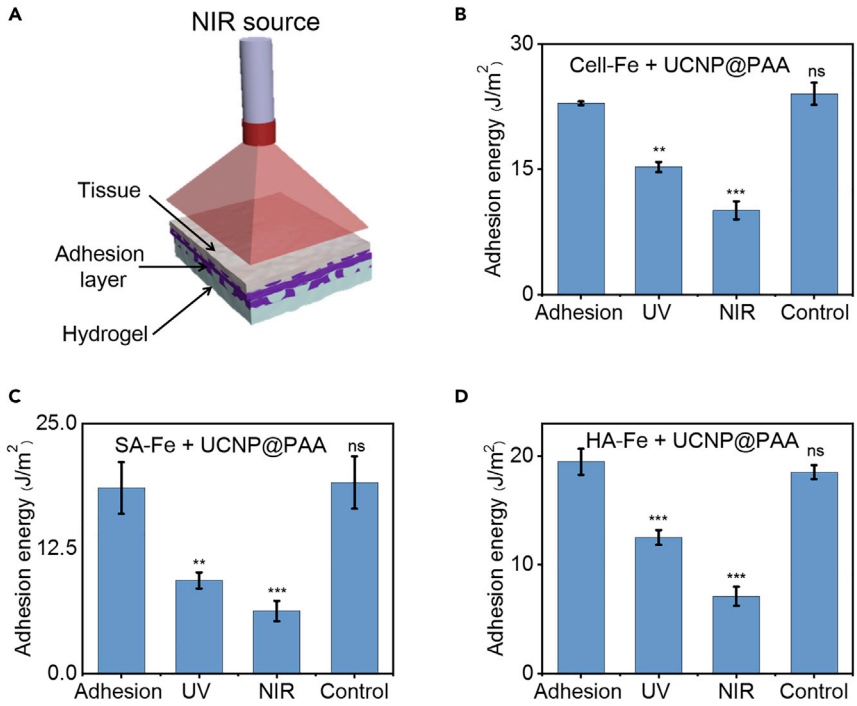

Figure 4. NIR-Detached Adesion Assisted by UCNP@PAA in the Deep Tissue

(A) Schematic of NIR-triggered disruption of topological adhesion between a hydrogel and tissue.

(B–D) Strength of the topological adhesion between a hydrogel and tissue upon UV irradiation (5 min), NIR light irradiation (5 min), and without irradiation. UCNP@PAA: 3 mg/mL, Fe^{3+}: 0.25 mol/L, molar ratio of Fe^{3+}/citric acid = 2: 1, (B) Cell: 1 wt%; (C) SA: 1 wt%; (C) HA: 0.5 wt%.

*p < 0.05, **p < 0.005, ***p < 0.001, ns = no statistical difference. See also Figures S7, S9, and S10.

Topological adhesion disruption is of great importance in bio-medical fields. Thus, the as-developed PUTAD strategy was explored for disrupting the adhesion between tissue (3 mm) and a hydrogel. Before that, the biocompatibility of the PUTAD strategy was investigated. MTT assays showed that cell growth was not obviously inhibited when the concentration of the PUTAD formula (30% UCNP@PAA, 10% Cell, 40% Fe^{3+}, and 20% citric acid) reached 1,000 μg/mL (Figure S7). The biocompatibility of upconverted UV light was also evaluated by MTT assay. There is no obvious difference between the cellular viability with and without UCNP@PAA upon excitation of NIR light (Figure S9). These results demonstrated that the PUTAD strategy has good biocompatibility and can be used in biological systems. After that, topological adhesion between tissue and a hydrogel was achieved using a UCNP@PAA Cell-Fe composite. Subsequently, NIR radiation penetrated the tissue to photodetach the adherents (Figure 4A). The topological adhesion strength between the hydrogel and tissue decreased from ~22 to ~3 J m^{-2} upon NIR irradiation (Figure 4B). As a comparison, UV irradiation alone triggered a decrease in adhesion strength from ~22 to ~15 J m^{-2} (Figure 4B). In a control experiment, the adhesion strength did not obviously change upon NIR irradiation in the absence of UCNP@PAA (Figure 4B). To further demonstrate the general applicability of the as-developed PUTAD method, UCNP@PAA was combined with different topological adhesives including sodium alginate (SA)/Fe^{3+} and hyaluronic acid (HA)/Fe^{3+} (termed SA-Fe and HA-Fe, respectively) for hydrogel and tissue adhesion. Both of the topological adhesives (SA-Fe and HA-Fe) showed good biocompatibility (Figure S7). For all samples, the adhesive strengths did not show obvious changes without irradiation (Figures 4C and 4D). However, losses of ~63% and 86% of the adhesive strength was observed for the UCNP@PAA+SA-Fe and UCNP@PAA+HA-Fe samples, respectively (18 to 7 J m^{-2} and 20 to 6 J m^{-2}) (Figures 4C and 4D). UV-treated UCNP@PAA+SA-Fe and UCNP@PAA+HA-Fe only demonstrated losses of ~36% and ~30% of the adhesive strength, respectively (Figures 4C and 4D). These results demonstrated that, compared with UV light, NIR light more efficiently triggered detachment of the tissue and hydrogel after penetrating the tissue. To further demonstrate the safety and applicability of the as-developed PUTAD method, hydrogel hematoxylin-eosin (H&E) staining between tissue and hydrogel was performed. We conducted the detachment using NIR light between the hydrogel and skin of mice. The HE results showed that NIR-triggered detachment did not alter the skin tissue obviously (Figure S10). These results, combined with the results of cellular

experiment, confirmed the biosafety of our PUTAD strategy. This elegant photodetachment of topologically adhered surfaces in deep tissue makes the system broadly applicable in future bio-medical applications.

DISCUSSION

In summary, we developed a PUTAD method assisted by upconverting nanoparticles for achieving NIR-regulated detachment. Owing to the strong penetrating ability of NIR radiation, PUTAD can be applied in deep tissue, which makes it suitable for applications in bio-medical fields. Notably, although NIR-triggered photothermal effect in our study did not cause the side effect for the detachment, attention should still be paid for its future application. The NIR-triggered photothermal effect might be greatly suppressed and even eliminated using more efficient UCNPs or cooling setup. Actually, NIR light can trigger different photoreactions via upconverting nanoparticle-assisted process, such as photocleavage or photoisomerization. Thus, in the future, combining UCNPs and these photosensitive reactions might develop lots of potential NIR-regulated detachment between the wetting soft materials, tissue, or other bio-medical adherents. Thus, our method provides not only a platform for detaching topological coordination adhesion but also a general strategy for developing NIR-detachable adhesives.

Limitation of the Study

We have developed a PUTAD method assisted by upconverting nanoparticles for achieving NIR-regulated detachment. However, the adhesion was slow as the photodetachable adhesive Cell-Fe needed time to penetrate in hydrogel substrate and the interlinks could not form quickly. Instability of ionic cross-linking results in weak adhesion strengthen. To conquer this problem, the stable cross-linking covalent bond, which could be photocleaved, might be employed for the adhesion and photodetachment in the future.

METHODS

All methods can be found in the accompanying Transparent Methods supplemental file.

SUPPLEMENTAL INFORMATION

Supplemental Information can be found online at https://doi.org/10.1016/j.isci.2020.100832.

ACKNOWLEDGMENTS

This work was supported by the National Natural Science Foundation of China (31890770 and 31800494) and the Young Elite Scientists Sponsorship Program by CAST (2018QNRC001).

AUTHOR CONTRIBUTIONS

Z.C. and S.L. participated in the conception and design of the research. M.J. carried out the experiments and characterizations. Z.C., M.J., and X.L. prepared the figures and drafted the manuscript. J.L. and S.L. revised the manuscript.

DECLARATION OF INTERESTS

The authors declare no competing interests.

Received: October 16, 2019
Revised: December 18, 2019
Accepted: January 7, 2020
Published: February 21, 2020

REFERENCES

All, A.H., Zeng, X., Teh, D.B.L., Yi, Z., Prasad, A., Ishizuka, T., Thakor, N., Hiromu, Y., and Liu, X. (2019). Expanding the toolbox of upconversion nanoparticles for in vivo optogenetics and neuromodulation. Adv. Mater. *31*, e1803474.

Burks, P.T., Garcia, J.V., GonzalezIrias, R., Tillman, J.T., Niu, M., Mikhailovsky, A.A., Zhang, J., Zhang, F., and Ford, P.C. (2013). Nitric oxide releasing materials triggered by near-infrared excitation through tissue filters. J. Am. Chem. Soc. *135*, 18145–18152.

Carling, C.J., Boyer, J.C., and Branda, N.R. (2009). Remote-control photoswitching using NIR light. J. Am. Chem. Soc. *131*, 10838–10839.

Chan, E.M., Han, G., Goldberg, J.D., Gargas, D.J., Ostrowski, A.D., Schuck, P.J., Cohen, B.E., and Milliron, D.J. (2012). Combinatorial discovery of lanthanide-doped nanocrystals with spectrally pure upconverted emission. Nano Lett. *12*, 3839–3845.

Chen, G., Qiu, H., Prasad, P.N., and Chen, X. (2014a). Upconversion nanoparticles: design, nanochemistry, and applications in theranostics. Chem. Rev. *114*, 5161–5214.

Chen, Z., Zhou, L., Bing, W., Zhang, Z., Li, Z., Ren, J., and Qu, X. (2014b). Light controlled reversible inversion of nanophosphor-stabilized pickering

emulsions for biphasic enantioselective biocatalysis. J. Am. Chem. Soc. *136*, 7498–7504.

Chen, G., Damasco, J., Qiu, H., Shao, W., Ohulchanskyy, T.Y., Valiev, R.R., Wu, X., Han, G., Wang, Y., and Yang, C. (2015a). Energy-cascaded upconversion in an organic dye-sensitized core/shell fluoride nanocrystal. Nano Lett. *15*, 7400–7407.

Chen, Z., He, S., Butt, H.J., and Wu, S. (2015b). Photon upconversion lithography: patterning of biomaterials using near-infrared light. Adv. Mater. *27*, 2203–2206.

Chen, Z., Xiong, Y., Etchenique, R., and Wu, S. (2016). Manipulating pH using near-infrared light assisted by upconverting nanoparticles. Chem. Commun. (Camb.) *52*, 13959–13962.

Gao, H.D., Thanasekaran, P., Chiang, C.W., Hong, J.L., Liu, Y.C., Chang, Y.H., and Lee, H.M. (2015). Construction of a near-infrared-activatable enzyme platform to remotely trigger intracellular signal transduction using an upconversion nanoparticle. ACS Nano *9*, 7041–7051.

Guimard, N.K., Oehlenschlaeger, K.K., Zhou, J., Hilf, S., Schmidt, F.G., and Barner-Kowollik, C. (2012). Current trends in the field of self-healing materials. Macromol. Chem. Phys. *213*, 131–143.

He, S., Krippes, K., Ritz, S., Chen, Z., Best, A., Butt, H.J., Mailänder, V., and Wu, S. (2015). Ultralow-intensity near-infrared light induces drug delivery by upconverting nanoparticles. Chem. Commun. (Camb.) *51*, 431–434.

Huang, K., Idris, N.M., and Zhang, Y. (2016). Engineering of lanthanide-doped upconversion nanoparticles for optical encoding. Small *12*, 836–852.

Kamperman, M., and Synytska, A. (2012). Switchable adhesion by chemical functionality and topography. J. Mater. Chem. *22*, 19390–19401.

Lederhose, P., Chen, Z., Mueller, R., Blinco, J.P., Wu, S., and Barner-Kowollik, C. (2016). Near-infrared photoinduced coupling reactions assisted by upconversion nanoparticles. Angew. Chem. Int. Ed. *55*, 12195–12199.

Li, J., and Mooney, D.J. (2016). Designing hydrogels for controlled drug delivery. Nat. Rev. Mater. *1*, 16071.

Li, C., Yang, D., Ma, P., Chen, Y., Wu, Y., Hou, Z., Dai, Y., Zhao, J., Sui, C., and Lin, J. (2013). Multifunctional upconversion mesoporous silica nanostructures for dual modal imaging and in vivo drug delivery. Small *9*, 4150–4159.

Li, W., Wang, J., Ren, J., and Qu, X. (2014). Near-infrared upconversion controls photocaged cell adhesion. J. Am. Chem. Soc. *136*, 2248–2251.

Li, J., Celiz, A., Yang, J., Yang, Q., Wamala, I., Whyte, W., Seo, B., Vasilyev, N., Vlassak, J., and Suo, Z. (2017). Tough adhesives for diverse wet surfaces. Science *357*, 378–381.

Luo, X., Lauber, K.E., and Mather, P.T. (2010). A thermally responsive, rigid, and reversible adhesive. Polymer *51*, 1169–1175.

Ruggiero, E., Habtemariam, A., Yate, L., Mareque-Rivas, J., and Salassa, L. (2014). Near infrared photolysis of a Ru polypyridyl complex by upconverting nanoparticles. Chem. Commun. (Camb.) *50*, 1715–1718.

Steck, J., Yang, J., and Suo, Z. (2019). Covalent topological adhesion. ACS Macro Lett. *8*, 754–758.

Stepuk, A., Mohn, D., Grass, R.N., Zehnder, M., Krämer, K.W., Pellé, F., Ferrier, A., and Stark, W.J. (2012). Use of NIR light and upconversion phosphors in light-curable polymers. Dent. Mater. *28*, 304–311.

Strehmel, B., and Strehmel, V. (2007). Two-photon physical, organic, and polymer chemistry: theory, techniques, chromophore design, and applications. Adv. Photochem. *29*, 111–354.

Sun, T.L., Kurokawa, T., Kuroda, S., Ihsan, A.B., Akasaki, T., Sato, K., Haque, M.A., Nakajima, T., and Gong, J. (2013). Physical hydrogels composed of polyampholytes demonstrate high toughness and viscoelasticity. Nat. Mater. *12*, 932.

Tian, G., Ren, W., Yan, L., Jian, S., Gu, Z., Zhou, L., Jin, S., Yin, W., Li, S., and Zhao, Y. (2013). Red-emitting upconverting nanoparticles for photodynamic therapy in cancer cells under near-infrared excitation. Small *9*, 1929–1938.

Viger, M.L., Grossman, M., Fomina, N., and Almutairi, A. (2013). Low power upconverted near-IR light for efficient polymeric nanoparticle degradation and cargo release. Adv. Mater. *25*, 3733–3738.

Wang, X., Valiev, R.R., Ohulchanskyy, T.Y., Ågren, H., Yang, C., and Chen, G. (2017). Dye-sensitized lanthanide-doped upconversion nanoparticles. Chem. Soc. Rev. *46*, 4150–4167.

Wu, S., and Butt, H.J. (2016). Near-infrared-sensitive materials based on upconverting nanoparticles. Adv. Mater. *28*, 1208–1226.

Wu, W., Yao, L., Yang, T., Yin, R., Li, F., and Yu, Y. (2011). NIR-light-induced deformation of cross-linked liquid-crystal polymers using upconversion nanophosphors. J. Am. Chem. Soc. *133*, 15810–15813.

Wu, X., Zhang, Y., Takle, K., Bilsel, O., Li, Z., Lee, H., Zhang, Z., Li, D., Fan, W., and Duan, C. (2016). Dye-sensitized core/active shell upconversion nanoparticles for optogenetics and bioimaging applications. ACS Nano *10*, 1060–1066.

Xu, D., Hawk, J.L., Loveless, D.M., Jeon, S.L., and Craig, S.L. (2010). Mechanism of shear thickening in reversibly cross-linked supramolecular polymer networks. Macromolecules *43*, 3556–3565.

Xu, J., Han, W., Cheng, Z., Yang, P., Bi, H., Yang, D., Niu, N., He, F., Gai, S., and Lin, J. (2018). Bioresponsive and near infrared photon co-enhanced cancer theranostic based on upconversion nanocapsules. Chem. Sci. *9*, 3233–3247.

Yan, B., Boyer, J.C., Branda, N.R., and Zhao, Y. (2011). Near-infrared light-triggered dissociation of block copolymer micelles using upconverting nanoparticles. J. Am. Chem. Soc. *133*, 19714–19717.

Yan, B., Boyer, J.C., Habault, D., Branda, N.R., and Zhao, Y. (2012). Near infrared light triggered release of biomacromolecules from hydrogels loaded with upconversion nanoparticles. J. Am. Chem. Soc. *134*, 16558–16561.

Yang, Y., Shao, Q., Deng, R., Wang, C., Teng, X., Cheng, K., Cheng, Z., Huang, L., Liu, Z., and Liu, X. (2012). In vitro and in vivo uncaging and bioluminescence imaging by using photocaged upconversion nanoparticles. Angew. Chem. Int. Ed. *51*, 3125–3129.

Yang, D., Hou, Z., Cheng, Z., Li, C., and Lin, J. (2015). Current advances in lanthanide ion (Ln 3+)-based upconversion nanomaterials for drug delivery. Chem. Soc. Rev. *44*, 1416–1448.

Yang, J., Bai, R., and Suo, Z. (2018). Topological adhesion of wet materials. Adv. Mater. *30*, 1800671.

Yu, J., Chary, S., Das, S., Tamelier, J., Pesika, N.S., Turner, K.L., and Israelachvili, J.N. (2011). Gecko-inspired dry adhesive for robotic applications. Adv. Funct. Mater. *21*, 3010–3018.

Zhao, L., Peng, J., Huang, Q., Li, C., Chen, M., Sun, Y., Lin, Q., Zhu, L., and Li, F. (2014). Near-infrared photoregulated drug release in living tumor tissue via yolk-shell upconversion nanocages. Adv. Funct. Mater. *24*, 363–371.

iScience, Volume *23*

Supplemental Information

Near-Infrared-Detached Adhesion Enabled by Upconverting Nanoparticles

Mingyue Jiang, Xue Liu, Zhijun Chen, Jian Li, Shouxin Liu, and Shujun Li

Supplemental Information

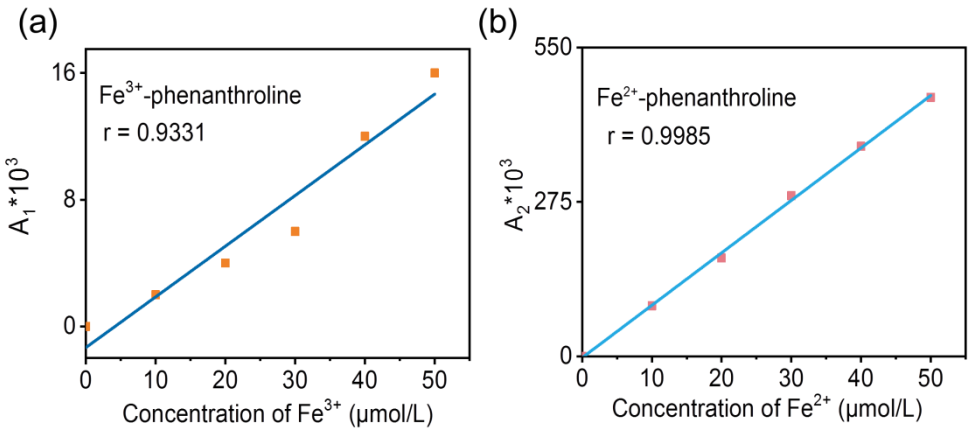

Figure S1 Calibration curves of absorbance vs. Fe ion concentrations in aqueous solutions; a) Fe^{3+} and b) Fe^{2+}. Related to **Figure 2**.

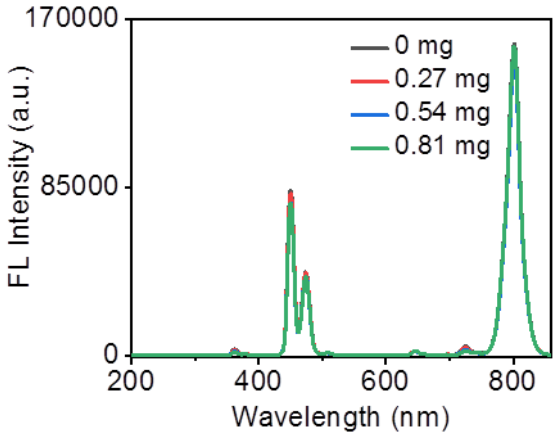

Figure S2 Fluorescence emission of UCNP@PAA (ranging from 200 nm-850 nm) upon addition of different amounts of Cell-Fe. Related to **Figure 2**.

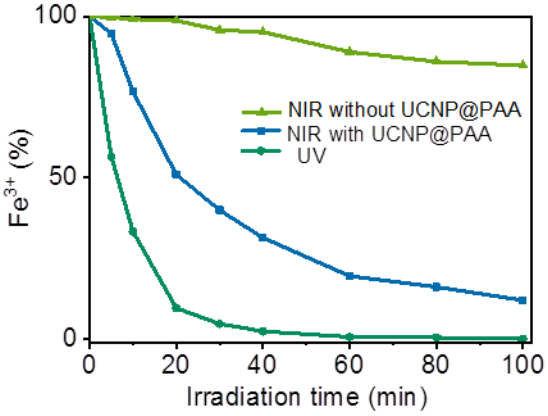

Figure S3 Changes in the Fe^{3+}/Fe^{2+} concentrations upon UV or NIR irradiation. Related to **Figure 2**.

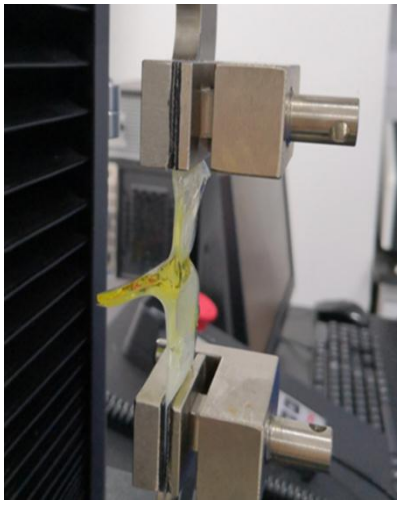

Figure S4 Photo of the peeling test without irradiation. Related to **Figure 3**.

Figure S5 Photo of the peeling test after NIR irradiation. Related to **Figure 3**.

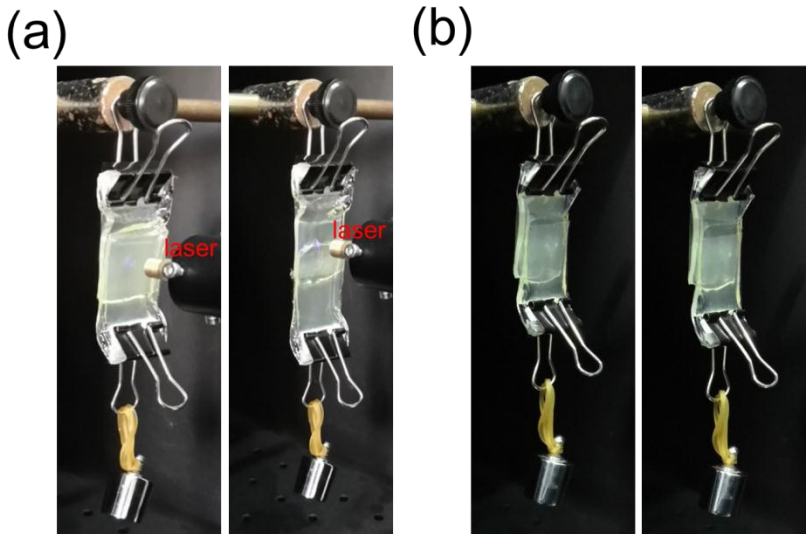

Figure S6 Photos of a weight was attached to the glued hydrogel. a) with NIR irradiation, beginning (left) and irradiated 1.5 min (right); b) without NIR irradiation, beginning (left) and after 10min (right). Related to **Figure 3**.

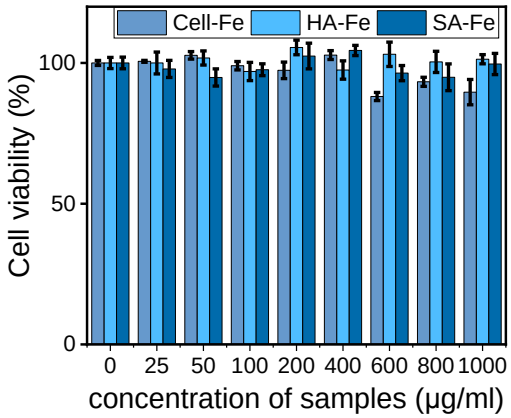

Figure S7 Cell viability values of L929 in the presence of UCNP@PAA + Cell-Fe, UCNP@PAA + SA-Fe and UCNP@PAA + HA-Fe at different concentrations. Related to **Figure 4**.

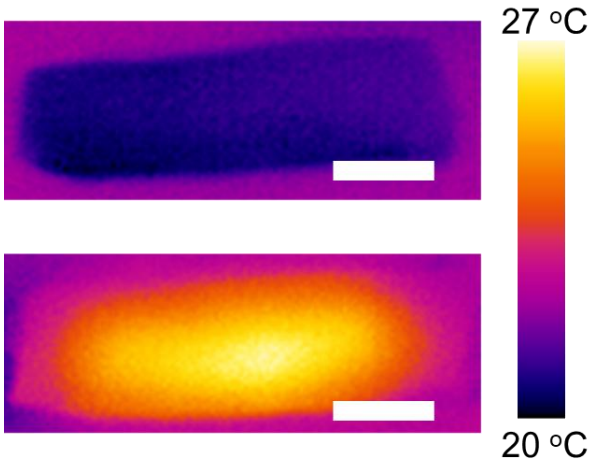

Figure S8 Infrared thermography of glued hydrogel with tissue before (top) and after (down) NIR irradiation for 5 min, scale bar = 1 cm. Related to **Figure 3**.

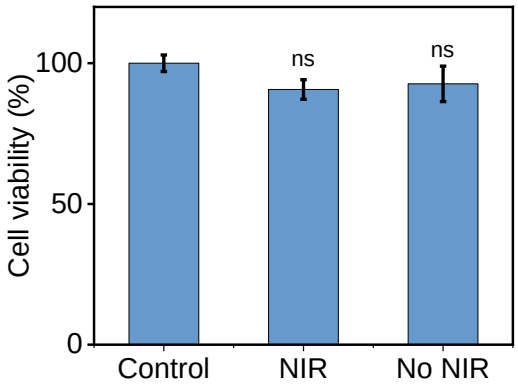

Figure S9 Cell viability of L929 in the presence of UCNP@PAA (300 µg/mL) upon NIR irradiation. *p < 0.05, **p < 0.005, ***p < 0.001, ns = no statistical difference. Related to **Figure 4**.

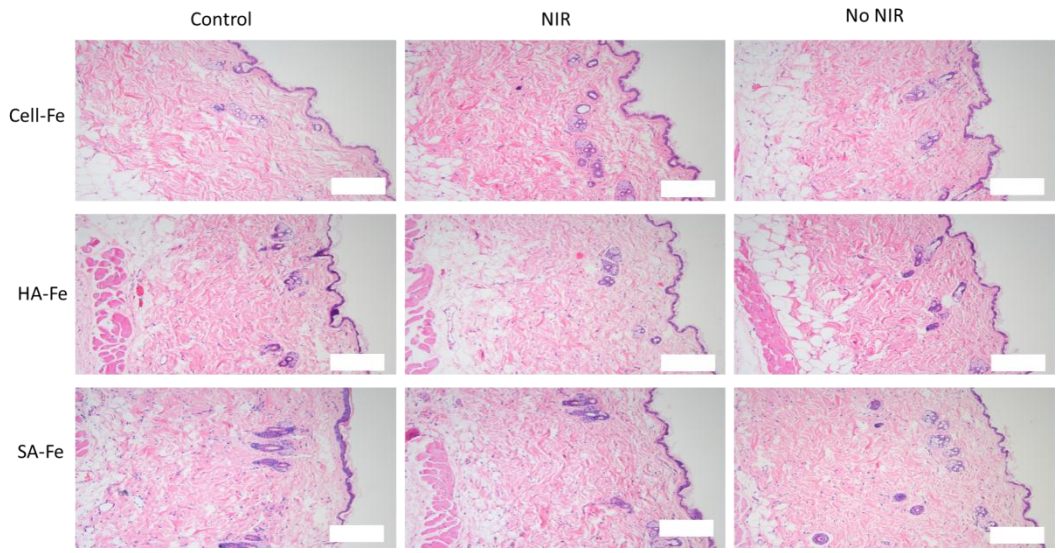

Figure S10 The images of mice skin and hydrogel hematoxylin-eosin (HE) staining. Scale bar = 50 um. Related to **Figure 4**.

Transparent Methods

Materials

All chemicals were purchased and used without further purification. All rare earth salts were purchased from Merck (Shanghai, China). Acrylamide (AAm; Sigma-Aldrich) was used to prepare the hydrogels. N,N'-Methylenebisacrylamide (MBAA; Sigma-Aldrich) was used as the crosslinker. Ammonium persulfate (APS; Sigma-Aldrich, A9164) and N,N,N',N'-tetramethylethylenediamine (TEMED) were used as the initiator and additive. Carboxymethylcellulose (Cell, *M*w = 9 W), citric acid monohydrate (C6O6H8·H2O), sodium alginate and ferric chloride hexahydrate (FeCl3·6H2O) were purchased from Aladdin and were used to prepare Cell-Fe. Hyaluronic acid was purchased from Macklin (Shanghai, China). 1,10-Phenanthroline, sodium acetate and hydroxylamine hydrochloride were purchased from Sinopharm Chemical Reagent Co., Ltd. and were used to determine the concentrations of ferric and ferrous ions.

Mice

Four-to six-week-old male or female mice were obtained from Beijing Vital River Laboratory Animal Technology Co., Ltd.

All procedures were conducted according to the Institutional Animal Care and Use Committee of the Model Animal Research Center. Animal experiments were approved by the Institute's Animal Ethics Committee of Northeast Forestry University.

Experimental Section

Characterization

UV−vis absorption spectra were acquired using a TU1901 spectrophotometer (Beijing Purkinje General Instrument Co., Ltd.). The mechanical properties were tested using a UTM2203

mechanical testing machine (Shenzhen Suns Technology Stock Co., Ltd.). Scanning electron microscopy (SEM) images were acquired using a JSM7500 scanning electron microscope (JEOL Ltd., Tokyo, Japan) at an accelerating voltage of 5.0 kV. Photoluminescence was measured using an *Omni*-λ 300i monochromator/spectrograph (Zolix, Beijing, China). A laser at 974 nm of MDL-N-974 (Changchun New Industries OptoelectronicsTechnology) coupled with a 105 μm (core) fiber was employed as the excitation source. Transmission electron microscopy (TEM) was conducted using a JEM2100 transmission electron microscope (JEOL Ltd., Tokyo, Japan) at an accelerating voltage of 200 kV.

Determination of Fe^{3+} and Fe^{2+} Concentration

We determined the concentrations of Fe^{3+} and Fe^{2+} ions in aqueous solutions according to a procedure reported in the literature (Peng et al, 2008). The Fe-phenanthroline system has a maximum absorbance at 510 nm, which was monitored with a TU1901 UV-Vis spectrophotometer at 25°C. We prepared 0~50 μmol/L Fe^{3+} solutions with 1,10-phenanthroline (0.06 wt%) and determined the absorbance of these solutions in sodium acetate buffer (0.1 mol/L). The absorbances of the Fe^{2+} solutions with the same concentrations as the Fe^{3+} solutions were recorded after adding a reducing agent (hydroxylamine hydrochloride (0.1 wt%)) into the above solutions. **Figure S1** shows the linear calibration curves of the absorbance against the concentrations of Fe^{3+} and Fe^{2+} ions.

The concentrations of Fe^{3+} and Fe^{2+} ions in the aqueous solutions of Cell-Fe was determined in the same way using the prepared calibration curves. The Fe^{3+}/citric acid complexing solution was diluted with ultrapure water, and 100 μL of UCNP@PAA (2 mg/mL) solution was added. After pretreatment, the absorbance of the mixed solution was recorded before and after NIR irradiation.

Transfer efficiency between UCNPs and Cell-Fe

The transfer efficiency between UCNPs and Cell-Fe was calculated according to the following equation:

$$\text{Transfer efficiency} = \frac{I_0 - I}{I_0} \times 100\% \qquad \text{Eq. S1}$$

I_o is the fluorescence emission intensity of UCNP@PAA at 365 nm, I is the fluorescence emission intensity of UCNP@PAA in the presence of Cell-Fe at 365 nm.

Preparation of the PAAm hydrogel

Acrylamide powder (13.52 g) was dissolved in deionized water (100 mL). Then, MBAA (MBAA to acrylamide weight ratio is 0.0006 :1) and TEMED (TEMED to acrylamide weight ratio is 0.0028 :1) were added. Next, APS (APS to acrylamide weight ratio is 0.01 :1) was added to the solution. The solution was mixed and degassed. The precursor solution was poured into a 2 mm thick plastic reaction vessel. Then, it was placed in a 60°C oven to air dry for 30 min and complete the polymerization.

Preparation of the NIR-detachable topological adhesives

The UCNP@PAA solution (3 mg/mL) was prepared in deionized water. An appropriate amount of Cell powder was dissolved in deionized water to form a 1 wt% Cell polymer aqueous

solution. A 1 wt% sodium alginate (SA) polymer solution was prepared by dissolving sodium alginate in deionized water. A 0.5 wt% HA polymer solution was prepared by dissolving hyaluronic acid in deionized water. The crosslinking solution for Cell, SA and HA was prepared with Fe^{3+}/citric acid complexing solution (C [Fe^{3+}] = 0.25 mol/L, the molar ratio of Fe^{3+} to citric acid is 2 :1). The pH of each mixture was adjusted to 3 by adding 10 mol/L NaOH dropwise and monitoring with a pH meter.

Topological adhesion of hydrogels

All the PAAm hydrogels were cut to a standard size of 70 mm × 20 mm × 2 mm. Then, 1 mL of Cell (1 wt%) aqueous solution was spread on the surface of two hydrogel samples, and the samples were left to stand for predetermined times to allow the solutions to penetrate the gel. After that, we wiped off the excess Cell solution using filter paper. Then, we spread 100 μL of Fe^{3+}/citric acid solution on one of the hydrogel surfaces and added 100 μL of UCNP@PAA solution at a certain concentration to the other. The two pieces of hydrogel were compressed together for 30 min.

Topological adhesion of porcine skin to hydrogels

The fresh porcine skin was purchased from a local market. First, the porcine skin was washed and immersed in deionized water at 37 °C for 2 h to remove the surface fat. Then, the porcine skin was cut into standard-sized pieces (70 mm × 20 mm × 3 mm). After that, 1 mL of 1 wt% Cell aqueous solution was spread on the surface of both porcine skin and PAAm hydrogel, and the samples were allowed to stand for a predetermined time to allow the solutions to penetrate the samples. Then, we spread 100 μL of Fe^{3+}/citric acid solution on the porcine skin and 100 μL of UCNP@PAA solution at a certain concentration on the PAAm hydrogel. Finally, these two substrates were pressed together with a certain strain for at least 30 min to achieve topological adhesion.

Peeling tests for measuring the adhesion energy

A 180° peeling test was used to measure the adhesion energy. The backs of the samples, which were of a standard size (70 mm × 20 mm × 2 mm), were taped with Scotch tape. The free ends of the samples were fixed to the tensile machine with a 100 N load cell. The peeling rate was fixed at 25 mm/min.

MTT Assay

Biocompatibility of upconverted UV light

L929 cells were seeded in a 96-well plate at a density of 1×10^4 cells per well and incubated for 24 h in an incubator containing 5% CO_2 at 37 °C. Then, the cells were incubated in fresh culture medium containing UCNP@PAA (300 μg/mL) for another 24 h. Then, the cells were exposed to the NIR light (NIR intensity = 4 W) for 5 min (pulse model, 50% frequency, period = 30 s), and the cells was incubated for 4 h continuously. After that, 50 μL of MTT solution (5 mg mL^{-1}) was added, and the cells were incubated for another 4 h. After removing the culture medium, 150 μL of DMSO was added to dissolve the formazan crystals. The absorbance of the solution at 490 nm was recorded, and the cell viability values were calculated according to

the following formula: cell viability (%) = the absorbance of the experimental group / the absorbance of control group × 100%.

Biocompatibility of topological adhesives

L929 cells were seeded in a 96-well plate at a density of 1×10^4 cells per well and incubated for 24 h in an incubator containing 5% CO_2 at 37 °C. Then, the cells were incubated in fresh culture medium containing different concentrations of UCNP@PAA + Cell-Fe (or UCNP@PAA + SA-Fe, or UCNP@PAA + HA-Fe) for another 24 h. Then, 50 μL of MTT solution (5 mg mL^{-1}) was added, and the cells were incubated for another 4 h. After removing the culture medium, 150 μL of DMSO was added to dissolve the formazan crystals. The absorbance of the solution at 490 nm was recorded, and the cell viability values were calculated according to the following formula: cell viability (%) = the absorbance of the experimental group / the absorbance of control group × 100%.

Hematoxylin-eosin (HE) staining

All the PAAm hydrogels were cut to a standard size of 10 mm × 10 mm × 2 mm. Then, 100 μL of Cell (1 wt%) aqueous solution was spread on the surface of hydrogel samples, and the samples were left to stand for predetermined times to allow the solutions to penetrate the gel. After that, excess Cell solution was wiped off the using filter paper. Then, 10 μL of Fe^{3+}/citric acid solution and 10 μL of UCNP@PAA solution were spread on the hydrogel surfaces. The hydrogels were put on the hairless mice which were anesthetized. After 30 min, the skin glued with hydrogel was irradiated for 5 min with NIR light. Then the skin was excised for hematoxylin-eosin (H&E) staining.

For hematoxylin-eosin (H&E) staining, previously reported methods were used in this experiment (Yang et al., 2017, Yang et al., 2016)**.** Briefly, the skin was excised and fixed in 4% (w/v) paraformaldehydebuffered saline and embedded in paraffin, 5 μm sections skin sections were cut and stained with H&E.

Supplemental References

Peng F., Li G., Liu X., Wu S., Tong Z.(2008). Redox-responsive gel-sol/sol-gel transition in poly(acrylic acid) aqueous solution containing Fe(III) ions switched by light. J. Am. Chem. Soc. *130*, 16166-16167

Yang Y., Lin L., Jing L., Yue X., Dai Z. (2017). CuInS2/ZnS quantum dots conjugating Gd (III) chelates for near-infrared fluorescence and magnetic resonance bimodal imaging. ACS Apll.Mater.Inter. *9*, 23450-23457.

Yang Y., Zhang J., Liu Z., Lin Q., Liu X., Bao C., Wang Y., Zhu L. (2016). Tissue‐integratable and biocompatible photogelation by the imine crosslinking reaction. Adv. Mater. *28*, 2724-2730.